

HONG KONG OBSERVATORY

Technical Note No. 100

SWIRLS - An Evolving Nowcasting System

by

P.W. Li W.K. Wong K.Y. Chan Edwin S.T. Lai

© Hong Kong Special Administrative Region Government

Published May 2000

Prepared by

Hong Kong Observatory
134A Nathan Road
Kowloon
Hong Kong

This publication is prepared and disseminated in the interest of promoting information exchange. The findings, conclusions and views contained herein are those of the authors and not necessarily those of the Hong Kong Observatory or the Government of the Hong Kong Special Administrative Region.

The Government of the Hong Kong Special Administrative Region (including its servants and agents) makes no warranty, statement or representation, express or implied, with respect to the accuracy, completeness, or usefulness of the information contained herein, and in so far as permitted by law, shall not have any legal liability or responsibility (including liability for negligence) for any loss, damage, or injury (including death) which may result, whether directly or indirectly, from the supply or use of such information.

Mention of product of manufacturer does not necessarily constitute or imply endorsement or recommendation.

Permission to reproduce any part of this publication should be obtained through the Hong Kong Observatory.

551.509

CONTENTS

	page
FIGURES	iv
1. INTRODUCTION	1
2. ECHO MOVEMENT AND TREC	2
3. RAINFALL RE-ANALYSIS AND FORECAST	4
4. OTHER SWIRLS APPLICATIONS	7
5. SWIRLS - THE NEXT GENERATION	8
ACKNOWLEDGEMENT	9
REFERENCES	10
APPENDICE I	11
II	12
III	13
IV	14

Abstract

A rainstorm nowcasting system SWIRLS (Short-range Warning of Intense Rainstorms in Localized Systems) is currently under development at the Hong Kong Observatory. One of the major components of the system is to make use of both radar and raingauge data to monitor and predict local rainfall distribution trends within the next couple of hours. Phase I of the development work has been completed and the system declared operational in April 1999. The major algorithms in SWIRLS developed are reported in this Technical Note. Selected cases are also used to illustrate the usefulness of SWIRLS in an operational environment and also to identify areas for future improvement.

摘要

天文台正發展一套名為『小渦旋』的臨近暴雨預報系統。此系統的其中一個主要部分是利用雷達和自動雨量計的資料監測和預測本地未來數小時的雨量分佈趨勢。第一階段的發展工作已經完成並在一九九九年四月正式投入業務運作。在這技術報告中我們將介紹『小渦旋』的主要計算程式，同時透過案例說明『小渦旋』在業務環境中的實用性，及指出一些需要改進的地方。

FIGURES

	page
1. Schematic diagram to show the computation of the TREC vector	15
2. TREC analysis of a squall line at 15:54 HKT on 2 May 1998	16
3. TREC analysis of Typhoon Victor at 19:00 HKT on 2 August 1997	17
4. TREC analysis of Typhoon Maggie at 4:00 HKT on 7 June 1999	18
5. Schematic diagram showing the calibration of radar reflectivity using real-time raingauge measurements	19
6. Flow diagram for the automatic radar-raingauge adjustment	20
7. Matching of 6-minute radar reflectivity data with 5-minute rain gauge data	21
8. Scattered plots of radar-raingauge analysis for a rainstorm case on 9 June 1998	22
9. One hour rainfall forecast by SWIRLS issued at 4:36 HKT on 9 June 1998 and the corresponding one hour rainfall accumulation over the raingauges from 4:40 HKT to 5:40 HKT on 9 June 1998	23
10. One hour rainfall forecast by SWIRLS for Typhoon Maggie issued at 3:30 HKT on 7 June 1999 and the corresponding one hour rainfall accumulation reported by the raingauges from 3:30 HKT to 4:30 HKT on 7 June 1999	24
11. Time series display of instability indices in TephViewer	25
12. Tephigram plot in TephViewer with capability for interactive adjustment	26
13. Synchronous display of radar products in RadarViewer	27
14. Complex interaction of echo groups on 9 June 1998 as revealed by the GTREC analysis	28

1. INTRODUCTION

The Hong Kong Observatory started a programme to develop a rainstorm nowcasting system SWIRLS (Short-range Warning of Intense Rainstorms in Localized Systems) in 1997. A SWIRLS prototype was put on operational trial in the rain season of 1998. The pilot experiment was considered to be a success with quantitative rainfall forecasts in the first couple of hours proving especially popular as an additional reference material for forecasters in operating the Rainstorm Warning System. Following some minor revisions based on users' input, Phase I of SWIRLS was officially declared operational in April 1999.

One of the main components in the first phase of SWIRLS is to make use of both radar and raingauge data to monitor and predict local rainfall distribution trends within the next couple of hours. The combined re-analyzed data set, based on a time-adjusted reflectivity-rainfall relationship, has proved to be extremely useful for provision of real-time rainfall information to the public and government decision-makers, formulation of nowcasting strategies, as well as for physical initialization in numerical weather prediction.

The main algorithms developed in Phase I, namely TREC and Quantitative Precipitation Forecast (QPF), are presented in this report. Other supporting SWIRLS applications, e.g. TephViewer and RadarViewer, are also introduced in brief. Throughout the discussion, selected cases are used to illustrate the usefulness of SWIRLS in an operational environment and also to identify areas for future improvement. More details on these cases and other articles related to SWIRLS can be found in the library in SWIRLS homepage on HKO Intranet. The report concludes with a discussion on the possible development strategies in the future phases of SWIRLS.

2. ECHO MOVEMENT AND TREC

Movement of individual radar echo between two consecutive CAPPI scans at 6-minute interval is derived using correlation method, i.e. TREC - Tracking Radar Echoes by Correlation. Cross-correlation technique was first used to determine the movement of the entire storm cluster (Hilst and Russo, 1960; Kessler and Russo, 1963; Crane, 1979; Bjerkaas and Forsyth, 1980). With the availability of higher resolution radar data, this technique was extended to retrieve the individual motion vectors of embedded storm cells (Rinehart and Garvey, 1978; Rinehart, 1979; Smythe and Zrnic, 1983; Tuttle and Foote, 1990).

The main advantage of using correlation method is that it requires only information from one single radar at two different observation times. Although the derived motion field is essentially two-dimensional in the horizontal and does not include strong vertical motion normally expected in convective cloud systems, the approximation should be good enough given that the effect of horizontal advection should be more pronounced if only short-term motion is considered. Once the motion vectors are computed, the entire echo field can be extrapolated to produce a short-term (say, one-hour) forecast field.

TREC method is applied to two successive CAPPI reflectivity fields at 6-minute interval. The first field (at time T_1) is divided into a number of equally sized "boxes" or two-dimensional arrays of pixels. The arrays of reflectivity values will then be cross-correlated with the arrays in the second field (at time $T_2 = T_1 + 6$ minutes). The correlation coefficient R is calculated using the following formula

$$R = \frac{\sum_k Z_1(k) \times Z_2(k) - \frac{1}{N} \sum_k Z_1(k) \sum_k Z_2(k)}{\left[\left(\sum_k Z_1^2(k) - N \overline{Z_1}^2 \right) \times \left(\sum_k Z_2^2(k) - N \overline{Z_2}^2 \right) \right]^{1/2}}$$

where Z_1 and Z_2 are the array of pixels of reflectivity at T_1 and T_2 respectively. The summation is carried out for all the data points and N is the total number of data points in the array. Computation can be repeated for all possible arrays found at T_2 to determine which array results in the highest correlation, and the centre of this second array will be the end point of motion vector (i.e. TREC vector). In practice, to reduce computation time, a search area centred on the first array is prescribed (Figure 1).

According to Tuttle and Foote (1990), the size of the "boxes" should be bounded by two considerations. A small "box" will contain too few data points for the correlation coefficients to be stable. A large "box" will only give the general mean flow on a broad spatial scale. In our study, the reflectivity field has a resolution of 480×480 pixels and the standard ranges of radar scan vary from 64 km, 128 km to 256 km. The array is set to have a fixed size of 19×19 pixels and thus the array size varies from 5 km (for 64km range of scan) to 20 km (for 256 km range of scan). The centres of pixel arrays are spaced 5 pixels apart and the whole TREC

vector field has a resolution of 93×93 . The search radius, which determines the expected maximum velocity of the echo motion, is usually set to be about the box width or it can be set according to sounding information.

Before the whole vector field is analyzed objectively, each motion vector has to pass a preliminary consistency check. If a TREC vector deviates more than 25 degree from the local mean of its neighbourhood (which is calculated from the set of 25 vectors located around it), it will be replaced by this mean vector. In this way, the "noisiness" as a result of sole consideration of maximum correlation in deriving the motion vector can be reduced at an early stage. To produce a continuous gridded vector field, a three-pass objective analysis using modified Cressman weighting function is then applied (see Appendix I).

The objective analysis is performed separately for the two components of the TREC vector field. The radius of influence can be set to arbitrary values in the three passes. For the TREC vector field of resolution 93×93 , the radius is set at 31 pixels, 16 pixels and 8 pixels for the first, second, and third pass respectively. This set of decreasing radius values is found to be most applicable in retaining the main features while giving a smooth and continuous field of TREC vectors on output.

The forecast radar reflectivity pattern is obtained by extrapolation based on the smoothed TREC vectors. Temporal integration makes use of the two-time-level semi-Lagrangian scheme (Staniforth and Cote, 1991). As the vector field is computed from consecutive radar CAPPI images six minutes apart, the integration scheme can output forecasts in 6-minute interval, and each successive forecast pattern is then used for the next step of integration.

The next issue relates to growth or decay in echo size and intensity. Echo intensity change is a result of many complex processes and close monitoring of echo development is essential for successful nowcasting. The TREC winds provide a basis to estimate the extent of growth and decay associated with each echo pixel. As the TREC vector traces the trajectory of individual echo, the difference in echo intensity along the flow between two successive radar scans can also be deduced. This information can be suitably included in the forecast if so desired.

Results from recent studies show that TREC is able to reproduce realistic wind fields associated with major weather systems. For example, the perturbed flow in the westerlies was well depicted in the travelling squall line on 2 May 1998 (Figure 2). For two typhoons that passed over Hong Kong on 2 August 1997 (Victor) and 7 June 1999 (Maggie), their wind circulations and asymmetric structures were both captured by TREC (Figures 3 and 4).

3. RAINFALL RE-ANALYSIS AND FORECAST

Apart from tracking the echoes and making a good short-range projection in movement and intensity, the amount of rain received at the surface remains the main forecasting issue. Conventionally, the Marshall-Palmer relationship is used in converting echo intensity (i.e. reflectivity, Z) to rainfall, R . But it is well known that the relationship is much generalized and does not apply well in many cases. To obtain a better estimate, SWIRLS makes use of raingauge data over Hong Kong to calibrate radar reflectivity in real time. In other words, the Z-R relationship will be adjusted in time as the rain event unfolds. If rain has not fallen as yet over any of the gauges and hence no ground truth available, the latest Z-R relationship from the last rain episode will be used as first guess.

To optimize the parameters a and b in the conventional $Z=aR^b$ relationship, radar reflectivity is correlated every five minutes with the rainfall recorded by the raingauges underneath. The adjusted Z-R relationship is used subsequently in the forecast module, based on TREC winds, to convert the forecast radar reflectivity into rainfall over the raingauge positions (Figure 5).

Various factors can affect the accuracy of the radar-rainfall estimation. Some of these factors are inherent in the radar beam characteristics and cannot be readily rectified. However, some studies such as Zawadzki *et al.* (1987) also suggest that sufficient accuracy in radar-rainfall estimation within a short distance (say, within 30 km from the radar) can still be achieved through a suitable choice of spatial and temporal resolution in the calculation. Based on the Zawadzki paper, the following procedure is adopted to adjust the Z-R relationship (Figure 6).

Radar CAPPI reflectivity images at 1-km height are used for the correlation exercise. The low altitude is chosen to be as close to the cloud base as practicable and hence more likely for the raindrops to preserve their volume on reaching the ground. Radar reflectivity data on polar coordinates are then converted into Cartesian coordinates for co-locations with the raingauge positions. Due to the presence of winds, falling raindrops will deviate horizontally from their starting positions. A search area from each raingauge position can be empirically adjusted to take this effect into account. Operationally, the default search area is defined to be within a distance of one pixel, i.e. over a 3 x 3 grid. The maximum intensity value within the search area, rather than intensity value averaged over the search area which is found to be less effective from investigative experiments, is assigned to the raingauge to form a potential radar-raingauge pair.

Figure 7 is a schematic highlighting the approaches adopted to circumvent the non-synchronous problem arising from the 6-minute radar volume scans and the 5-minute surface rainfall data measured by the tele-communicating automatic raingauges distributed over Hong Kong. Neglecting vertical air motion, a large spherical raindrop, say 5 mm in diameter, will

take about 1.5 minutes to reach the group from 1-km level. On the other hand, a small droplet of 1 mm in diameter can take up to 4 minutes to reach the ground from the same level. In other words, it will take a finite period of time for the surface gauge to collect all the rain associated with the observed radar echo. For a 6-minute radar sweep, the last arrivals could be as much as 10 minutes from the start time of the volume scan, i.e. roughly corresponding to two 5-minute gauge observations. As an illustration: for a radar scan that starts on the hour, say at 3:00 a.m., the small droplets picked up by the radar towards the end of the scan near 3:06 a.m. will reach the surface gauge at round about 3:10 a.m. As such, the radar image at 0300H (available at about 0310H after data processing) will be matched with the sum of the two latest observations from the raingauges, i.e. the sum of 5-minute rainfall ending at 0305H and 0310H (corresponding to Case 1 in Figure 7). Similarly for the radar image at 0330H, correlation will be against the sum of 5-minute rainfall ending at 0335H and 0340H (corresponding to Case 6 in Figure 7). In between the times of clock hour and half-past, details on the apportioning of weights between the two latest available gauge observations are as specified in Figure 7.

After some basic quality checks (see Appendix II), the radar-raingauge pairs are passed to a linear least square analysis for the determination of a and b , i.e.

$$\text{dBZ} = 10 \log a + b \text{ DBG}$$

where DBG is the raingauge rainfall expressed in decibel. To ensure statistical significance, all reporting radar-raingauge pairs, once accepted, will be retained for the linear least square analysis throughout the entire rain episode. Any departure of more than 2 standard deviation units from the best fit line will be discarded and the correlation will be re-calculated until a correlation coefficient of $r \geq 0.7$ is reached. Results have proven that the adopted approach is able to obtain reasonable Z-R relationship (Figure 8).

When there are not enough reporting radar-raingauge pairs, such as when a rainstorm is still outside Hong Kong, either the standard Marshall-Palmer relationship ($a = 200$, $b = 1.6$) or the Z-R relationship from the previous rain episode will be used. As more radar-raingauge pairs become available, the Z-R relationship will be updated accordingly.

Keeping things relatively simple to start with, there are basically three approaches in estimating short-term echo intensity changes: (a) assuming no change as from the latest scan; (b) assuming linear extrapolation from the latest scans; (c) imposing an idealized intensity profile upon the intensity trends as observed from the latest scans.

Option (a) may seem too simplistic but given the complexity of the problem, it has the advantage of providing forecasts with good continuity, or even reasonable estimates in some cases should rain generation and degeneration balance out on the broader scale. Option (b) in general gives reasonable extrapolation within the first hour. But given the short life cycle of convective cells, linear extrapolation will soon become unrealistic and rainfall forecasts based on such an assumption will soon become disproportionately large. Option (c) provides a possible,

though crude, remedy by imposing an idealized empirical intensity profile for rainfall forecasts. In the first phase of SWIRLS, option (a), i.e. no echo development, is included as reference for both 1-hour and 2-hour rainfall forecasts. For echo development, several profiling schemes, including option (b) and variations on option (c), are encoded in the QPF algorithms (see Appendix III). The operational scheme in use is Scheme 4, but will revert to Scheme 2 if only two consecutive radar observations are available.

Preliminary operational experience in the rain seasons of 1998 and 1999 suggests that reasonable rainfall forecasts can be achieved within the first two hours as long as the advective process is dominant and there is no volatile fluctuation in echo intensity, such as in the cases of a heavy rainstorm and tropical cyclone rainbands shown in Figures 9 and 10, respectively.

4. OTHER SWIRLS APPLICATIONS

A frequently updated rainfall distribution map based on the radar-raingauge re-analysis is included in the SWIRLS interface for forecasters' information. To edit the map, for reasons such as exclusion of incorrect data or better contouring effect, forecasters can interactively adjust the rainfall amount in specific locations as appropriate.

Two other applications, namely TephViewer and RadarViewer, are also made available in the first phase of SWIRLS to assist forecasters in assessing potential or developing rainstorm scenarios.

There are two streams of products within the TephViewer. A collection of often used instability indices, including actual observations as analyzed from soundings and predicted values as deduced from NWP models, are displayed in time series for forecasters' reference (Figure 11). Forecasters can, at a glance, assess the prevailing trends in atmospheric stability, as well as compare predicted figures against actual observations to evaluate model performance and reliability. In the tephigram plotting of the latest soundings (Figure 12), forecasters can interactively adjust the temperature and dew point profiles by clicking and dragging at the observation points. The corresponding instability indices will be automatically updated and displayed at the same time, thereby providing an indication on the overall effect such adjustments have on atmospheric stability. The idea is that through such man-machine interaction, the atmosphere's sensitivity to probable changes, either as suggested by real-time near-surface observations or as implied by NWP models, and hence the risks of convection triggering can be more effectively monitored.

As for the RadarViewer, it has the capability of displaying up to six different radar products synchronously (Figure 13). This can be an extremely useful tool when forecasters need to compare, assimilate and reconcile various kinds of radar information, e.g. rainfall rate, Doppler velocity, VIL, etc., in a short period of time. If proved popular, this viewer will be extended to incorporate and display other SWIRLS-related products in the next phase of SWIRLS.

5. SWIRLS - THE NEXT GENERATION

In performing TREC on individual echo movement, we realize the resultant wind field reflects probably only the prevailing low-level flow. The rainstorm system as a whole, linked to some mesoscale perturbations, often moves at an angle to the general flow. To address the problem, the correlation method is extended to the tracking of echo groups (i.e. GTREC - Group Tracking of Radar Echoes by Correlation - see Appendix IV for a brief overview). The objective is to depict system movement and to resolve the interaction of multiple systems. As an example, the rainstorm case on 9 June 1998 had a perturbation in the westerlies moving in from the west, sweeping over a quasi-stationary convergence line lying just off the coast of eastern Guangdong (Figure 14). The overall effects of such an interaction, especially the possibility of enhanced precipitation at the merging or intersecting point which would impact on the quantitative precipitation forecast, require more sophisticated treatment.

The GTREC approach is only one among the many options to be explored in the next generation(s) of SWIRLS. Already, plans for Phase II have been drawn up. From the experience gained in Phase I, we feel that we need to re-organize our development resources and home in on two major aspects: TRASER (Tracking of Radar And Satellite Estimated Rain) and REGrADe (Radar Echoes Growth And Decay). The former, incorporating satellite information along approaches similar to TREC and radar-raingauge QPF, will serve to extend forecast validity to probably up to six hours. The latter will focus on adding intensity change options, including methodologies based pattern recognition, terrain correction and real-time intensity profile, in an attempt to improve QPF in the first couple of hours. In parallel, a CSI (Critical Success Index) algorithm will be implemented to provide an objective measure of SWIRLS performance as more and more QPF options become available for forecasters to pick and choose.

Looking further afield, we also aim to explore the possibility of LAMAS (Local And Mesoscale Analysis System). For TRASER and REGrADe, no matter how successful, we can only be wise after the event. But LAMAS will enable us to look at convection or rainstorm precursors, especially with respect to local convergence effect under various synoptic situations. The pursuit of LAMAS, however, would involve the development of a storm scale numerical model in tandem. Given the dense observation available in Hong Kong and neighbouring Guangdong, it is a realistic challenge to be taken up and explored if we so wish.

ACKNOWLEDGEMENT

The authors are grateful to Mr. C.Y. Lam for his valuable comments and suggestions on this report.

REFERENCES

1. Benjamin, S.G., and N.L. Seaman 1985 A simple scheme for objective analysis in curved flow. *Mon. Wea. Rev.*, **113**, 1184-1198
2. Bjerkaas, C.L., and D.E. Forsyth 1980 Operational test of a three-dimensional echo tracking program. *Preprints 19th Conf. Radar Meteorology* Miami Beach, Amer. Meteor. Soc., 244-247
3. Crane, R.K. 1979 Automatic cell detection and tracking. *IEEE Trans. Geosci.Electron.*, **GE-17**, 250-262
4. Cressman, G.P. 1959 An operational objective analysis system. *Mon. Wea. Rev.*, **87**, 367-374
5. Hilst, G.R., and J.A. Russo, Jr. 1960 An objective extrapolation technique for semi-conservative fields with an application to radar patterns. Tech. Memo. No. 3, Travelers Weather Research Centre, Hartford, CT
6. Inman, R.L. 1970 Operational objective analysis schemes at the National Severe Storms Laboratory. Tech. Cir. No. 10, NSSL, ESSA, Norman, OK 73069, 91pp
7. Kessler, E., III, and J.A. Russo, Jr. 1963 Statistical properties of weather echoes, *Preprints 10th Weather Radar Conf.*, Washington, DC, Amer. Meteor. Soc., 25-33
8. Rinehart, R.E. 1979 Internal storm motions from a single non-Doppler weather radar. NCAR/TN-146+STR, 262pp
9. Rinehart, R.E. and E.T. Garvey 1978 Three-dimensional storm motion detection by conventional weather radar. *Nature*, **273**, 287-289
10. Smythe, G.R. and D.S. Zrnic 1983 Correlation analysis of Doppler radar data and retrieval of the horizontal wind. *J. Climate and Appl. Meteor.*, **22**, 297-311
11. Staniforth, A. and J. Cote 1991 Semi-Lagrangian integration schemes for atmospheric models - a review. *Mon. Wea. Rev.*, **119**, 2206-2223
12. Tuttle, J.D. and G.B. Foote 1990 Determination of the Boundary Layer Airflow from a Single Doppler Radar. *J. Atmos. Ocean. Tech.*, **7**, 218-232
13. Zawadzki, I., C. Desrochers and E. Torlaschi 1986 A Radar-raingauge Comparison. *Preprints, 23rd Conf. on Radar Meteorology*, Snowmass, Colorado, Amer. Meteor. Soc., 121-124

APPENDIX I

Objective Analysis of Vector Field

To produce a continuous field pattern and a gridded vector field, a three-pass objective analysis using modified Cressman weighting function is carried out.

Given an observed scalar field $s(i, j)$ (in this case it is one of the components of the TREC vector field derived from above procedures) and its first guess field $s_o(i, j)$, the corrected value $s^*(i, j)$ at each pass of the objective analysis can be found from the following relation,

$$s^*(i, j) = s_o(i, j) + \Delta s(i, j)$$

where,

$$\Delta s(i, j) = \frac{\sum_k w(i, j, k)^2 \times \Delta s(k)}{\sum_k w(i, j, k)}$$

and $\Delta s(k)$ = difference at observation point k (observed value minus first guess value),

$w(i, j, k)$ = modified Cressman weighting function at point (i, j) for the observation point k ,
(the summation is carried out over all observation points with positive weighting values).

The modified Cressman weighting function, which takes the derived TREC wind values into consideration, is an elliptic weighting function dependent on the distance and also the wind velocity between the observation and analysis points. The deformed shape from the traditional isotropic weighting function (Cressman, 1959) assigns a bigger weight to the adjustment of the whole field along the direction of flow. Inman (1970) proposed a form of such weighting function; Benjamin and Seaman (1985) improved it for general applicability, in a similar form as the isotropic Cressman weighting function,

$$w(i, j, k) = \begin{cases} \frac{R^2 - d_m^2}{R^2 + d_m^2} & \text{if } d_m^2 < R^2 \\ 0 & \text{if } d_m^2 > R^2 \end{cases}$$

where d_m is a function of distance of the observation from analysis points and also the observed velocity values.

APPENDIX II

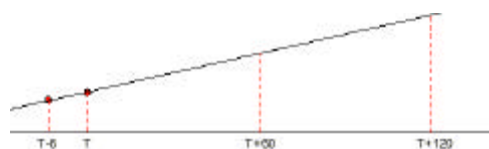
Raingauge Data Pre-processing

Raingauge data are pre-processed in the following steps before they are accepted for correlation with radar reflectivity data:

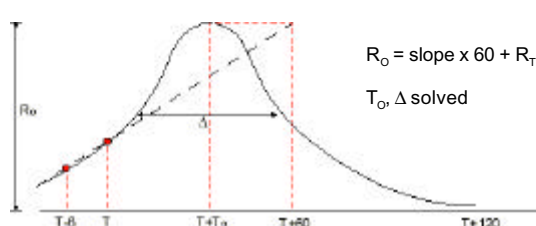
- (i) A range of values is prescribed for the 5-minute raingauge data. The upper bound is set to be 20 mm, corresponding to an intense rainstorm event with rainfall rate of 240 mm/hr. The lower bound is set to be 1 mm, corresponding to a rainfall rate of 12 mm/hr.
- (ii) The specified search area of radar echoes from individual gauge is set to be the distance of one pixel, i.e. a 3 x 3 grid with the gauge at the centre. The current default is to adopt the maximum reflectivity value among the nine selected pixels for correlation with rainfall recorded at the gauge. Investigative experiments have shown that for localized intense rainstorm, the maximum value approach is more sensitive to the severity of the situation. For moderate rain event, the average value approach can smooth out some signal fluctuations and seems to be more reasonable.
- (iii) The accepted radar-raingauge pairs are passed to the linear least square subroutine for determination of the correlation coefficients. To ensure significant statistics, more than 5 radar-raingauge pairs are required to start the correlation process. Otherwise, the rainfall analysis module will be terminated and the previous Z-R relationship will be adopted as first guess.
- (iv) Any radar-raingauge pair departing more than 2 standard deviation units from the best fit lines will be rejected. Through this procedure, outliers such as raingauges in the blind sectors of the radar beam are automatically removed.

APPENDIX III

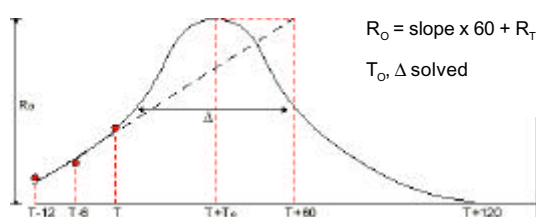
Echo tendency profiling scheme



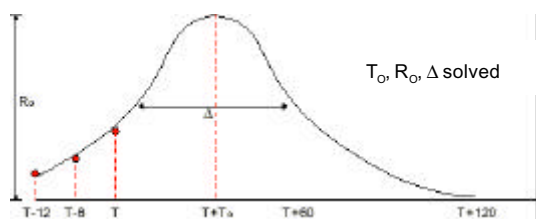
Scheme 1 Using reflectivity data at T and T-6 minutes, calculate echo intensity change along TREC trajectory. Projected intensity values are based on a linear trend.



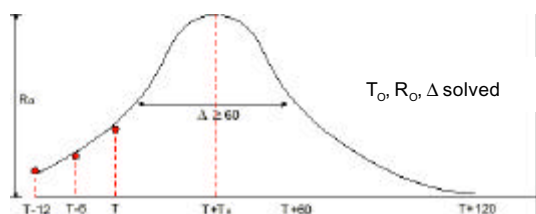
Scheme 2 Using reflectivity data at T and T-6 minutes, calculate echo intensity change along TREC trajectory. T+60 minute intensity based on linear extrapolation is taken as the peak value (amplitude) of a fitted Gaussian profile. From the slope and reflectivity values at T, the centre and width (i.e. between half-peak values) of the Gaussian profile are derived.



Scheme 3 Similar to Scheme 2 but the initial linear trend is derived from a best fit line through reflectivity values at T, T-6 and T-12 minutes. The weight is unity at T and decreases exponentially for T-6 and T-12 minutes. The centre and width of the Gaussian profile come from the slope and intercept values of the best fit line.



Scheme 4 For rainfall rate at T greater than 40 mm per hour, the second derivative of echo intensity with respect to time is calculated using data at T, T-6 and T-12 minutes. Amplitude, width and centre of the fitted Gaussian profile are derived from the slope of the best fit line and the intensity value at T. For rainfall rate smaller than 40 mm per hour, Scheme 3 is used.



Scheme 5 Similar to Scheme 4 but for those profiles with width less than 60 minutes, reset width to 60 minutes and re-compute corresponding amplitude and centre of Gaussian profile.

Appendix IV

GTREC (Group Tracking of Radar Echoes by Correlation)

While TREC focuses on pixel-scale movement, GTREC tracks the movement of echo groups with the help of a storm cell identification algorithm (i.e. cell-scale movement). This identification algorithm uses successive reflectivity CAPPI images to compute: (1) the locations of echo groups, (2) their movement over the past 30 - 60 minutes, and (3) short-term forecast of storm cell positions. Other cell-based information such as position and intensity can also be computed for display purpose as well as for further development work.

Reflectivity CAPPI images of various range (64 km - 256 km) at different altitudes can be used to identify the 2-dimensional storm cells. Several radar reflectivity threshold levels (from 30 dBZ up to about 55 dBZ) are used to compute the cells in three major steps:

- (v) Label the segments of pixels in each pixel row with reflectivity values greater than the pre-defined threshold value.
- (vi) Check all these segments to see if they are adjacent to each other. If so, they are grouped together to form a "cell".
- (vii) Compute the cell parameters - the arithmetic and weighted mean positions, average cell intensity, maximum intensity, the derived geometric parameters after ellipse fitting (e.g. the length and inclination of major and minor axes).

The fitted ellipses can be readily displayed on SWIRLS application software and history of past movement shown in lines and dots. Continuity is maintained by searching all possible cell positions in the previous image within a maximum allowable range and identifying the nearest cell with similar group parameters (i.e. minimum change in time). GTREC vectors are then the displacement of centroids of ellipses between successive images. Short-term forecast of cell movement can be made by linear extrapolation.

If no "similar" cells are found within the search area, the algorithm will consider the possibility of merging and splitting. For example, for the merging case, the ellipse will be displaced along its minor axis in the direction of a "not-so-similar" and smaller cell in the proximity identified in the previous image. Other smaller cells in the previous image coming under the coverage of the displaced ellipse will then be considered as merging candidates. A similar but reverse process will be carried out for the splitting case.

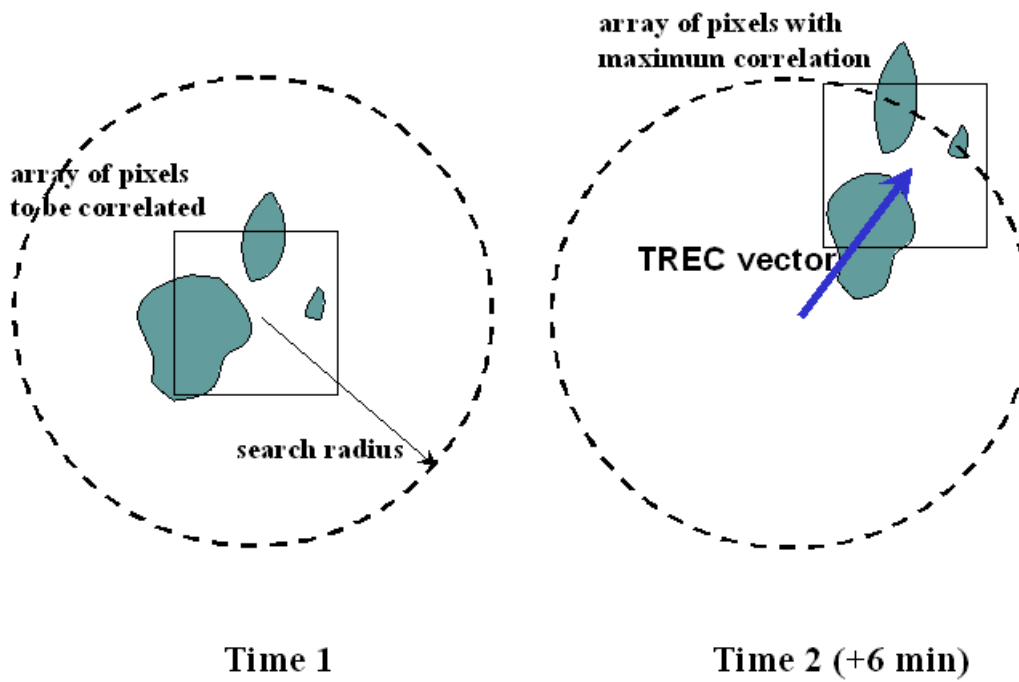


Figure 1 Schematic diagram showing the computation of the TREC vector to find the motion of reflectivity echoes (shaded). The pixel array at Time 1 is correlated with all pixel arrays of the same size within the searching radius at Time 2. The centre of the array at Time 2 with maximum correlation coefficient designates the end point of the TREC vector.

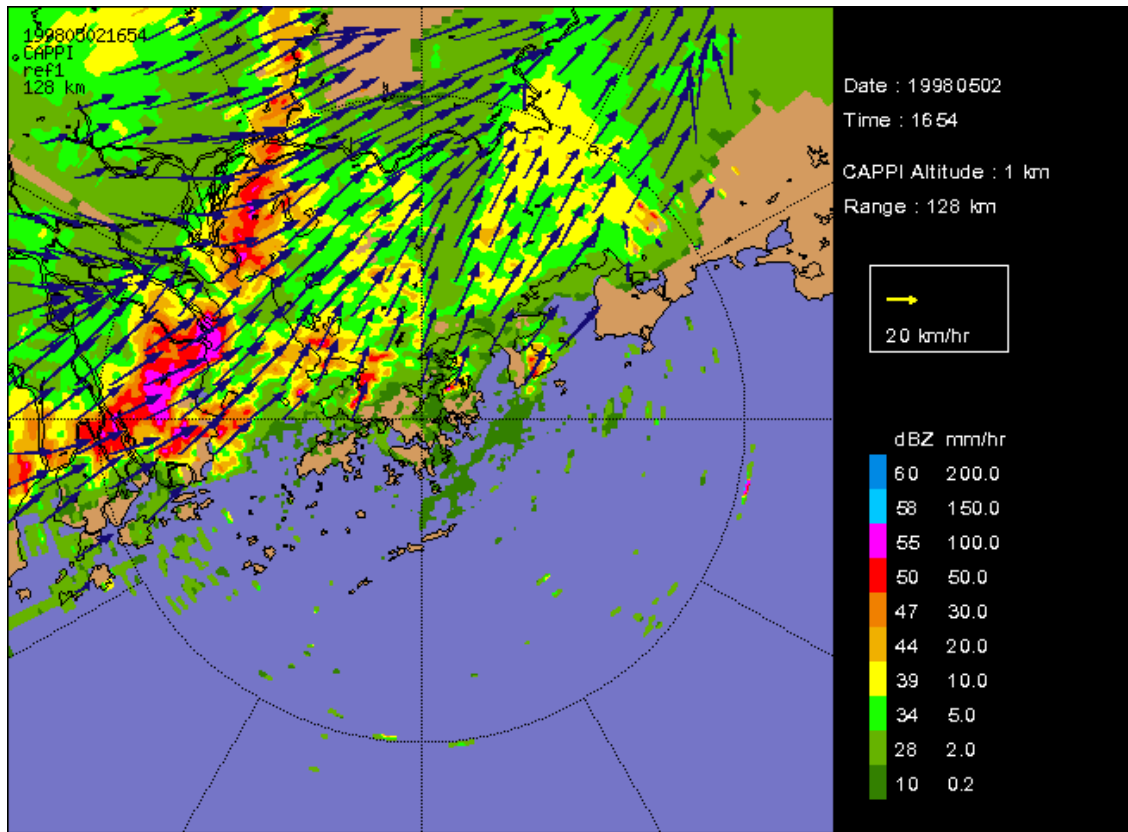


Figure 2 TREC analysis of a squall line approaching Hong Kong from the northwest at 15:54 HKT on 2 May 1998.

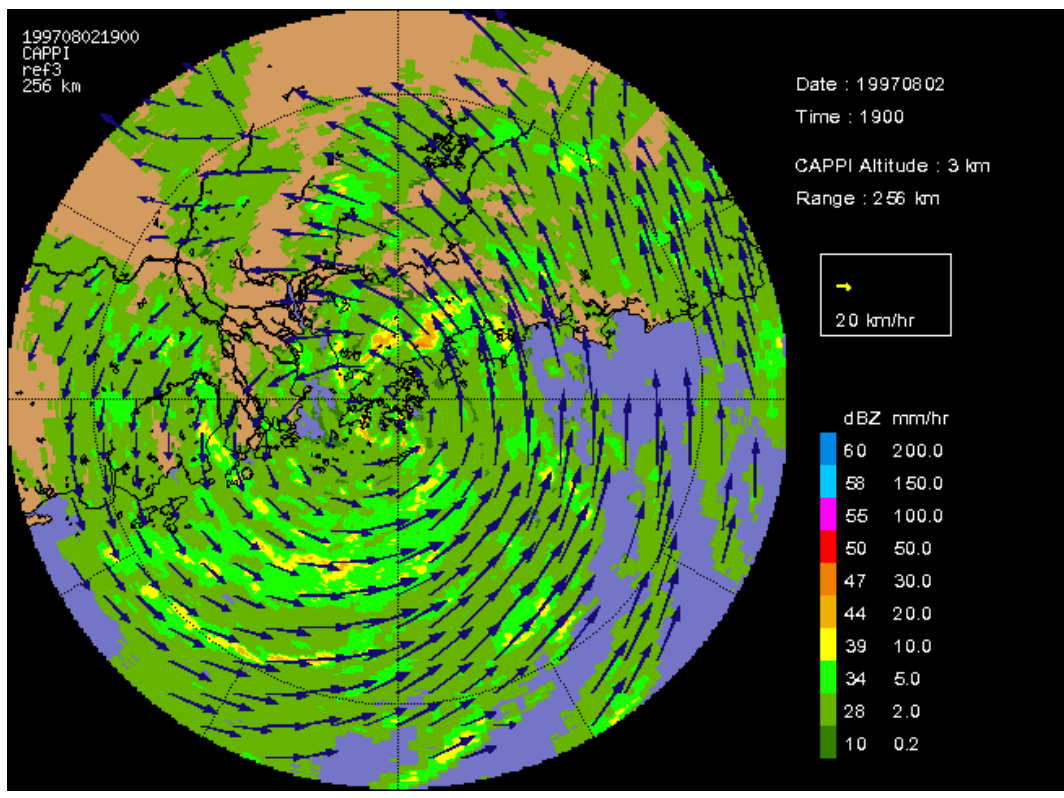


Figure 3 TREC analysis of Typhoon Victor (9712) over Hong Kong at 19:00 HKT on 2 August 1997.

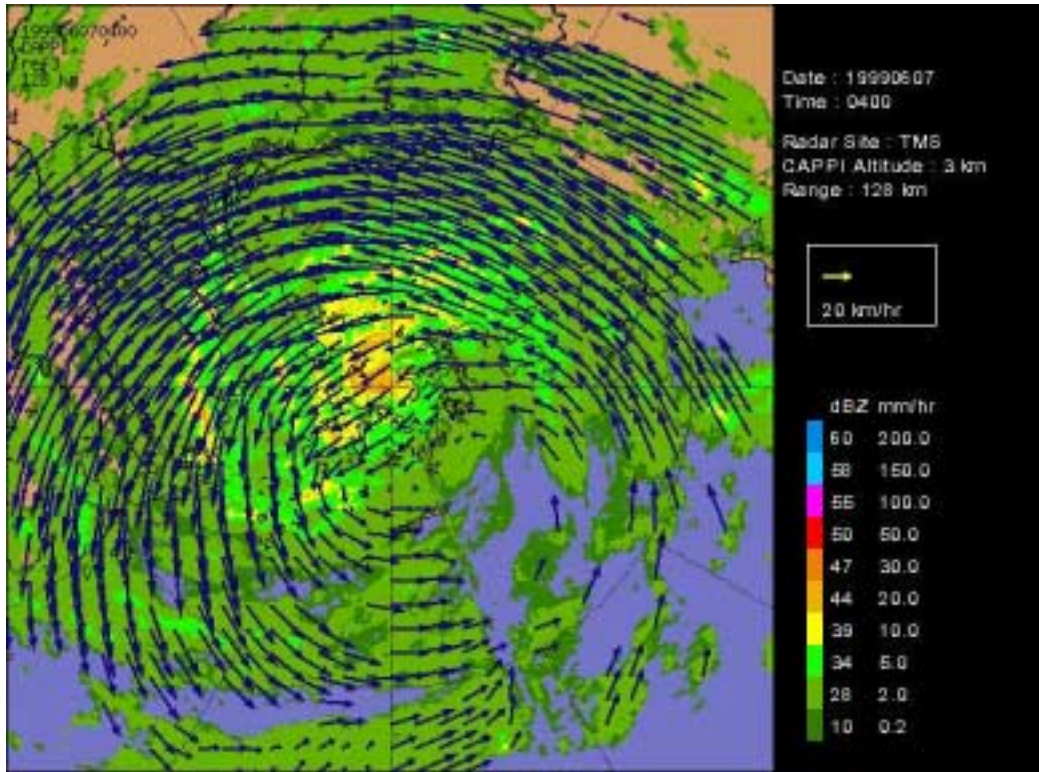


Figure 4 TREC analysis for Typhoon Maggie (9903) over Hong Kong at 4:00 HKT on 7 June 1999.

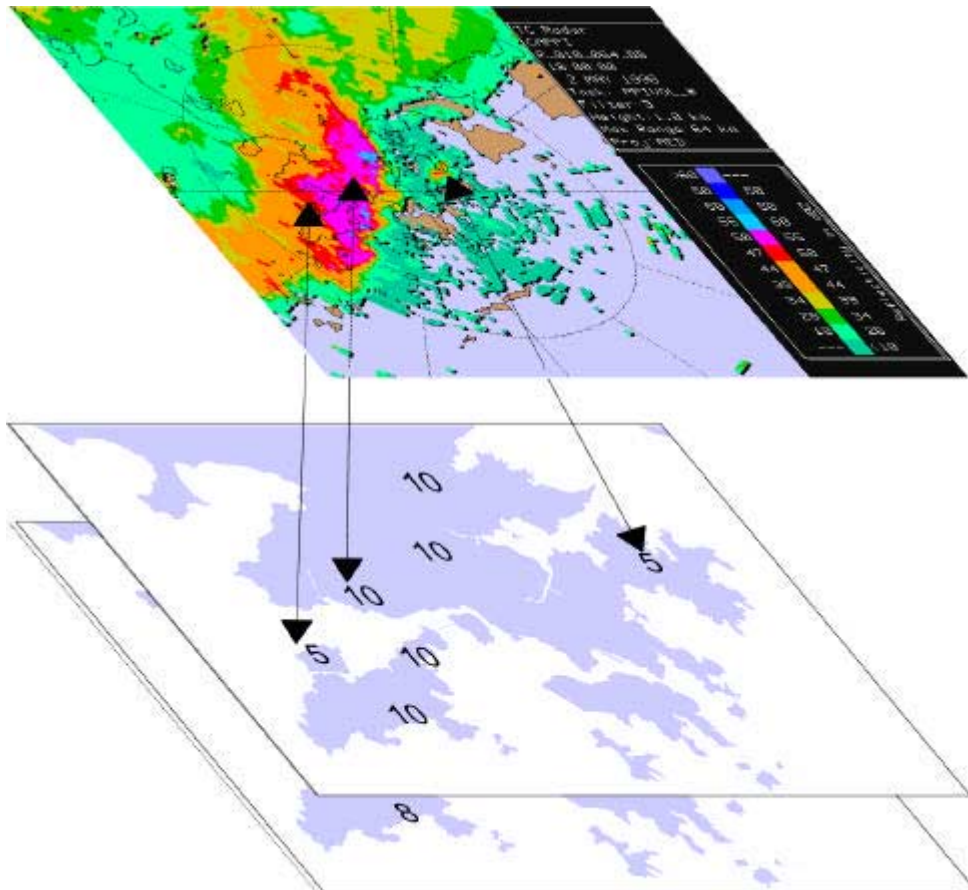


Figure 5 Schematic diagram showing the calibration of radar reflectivity using real-time raingauge measurements.

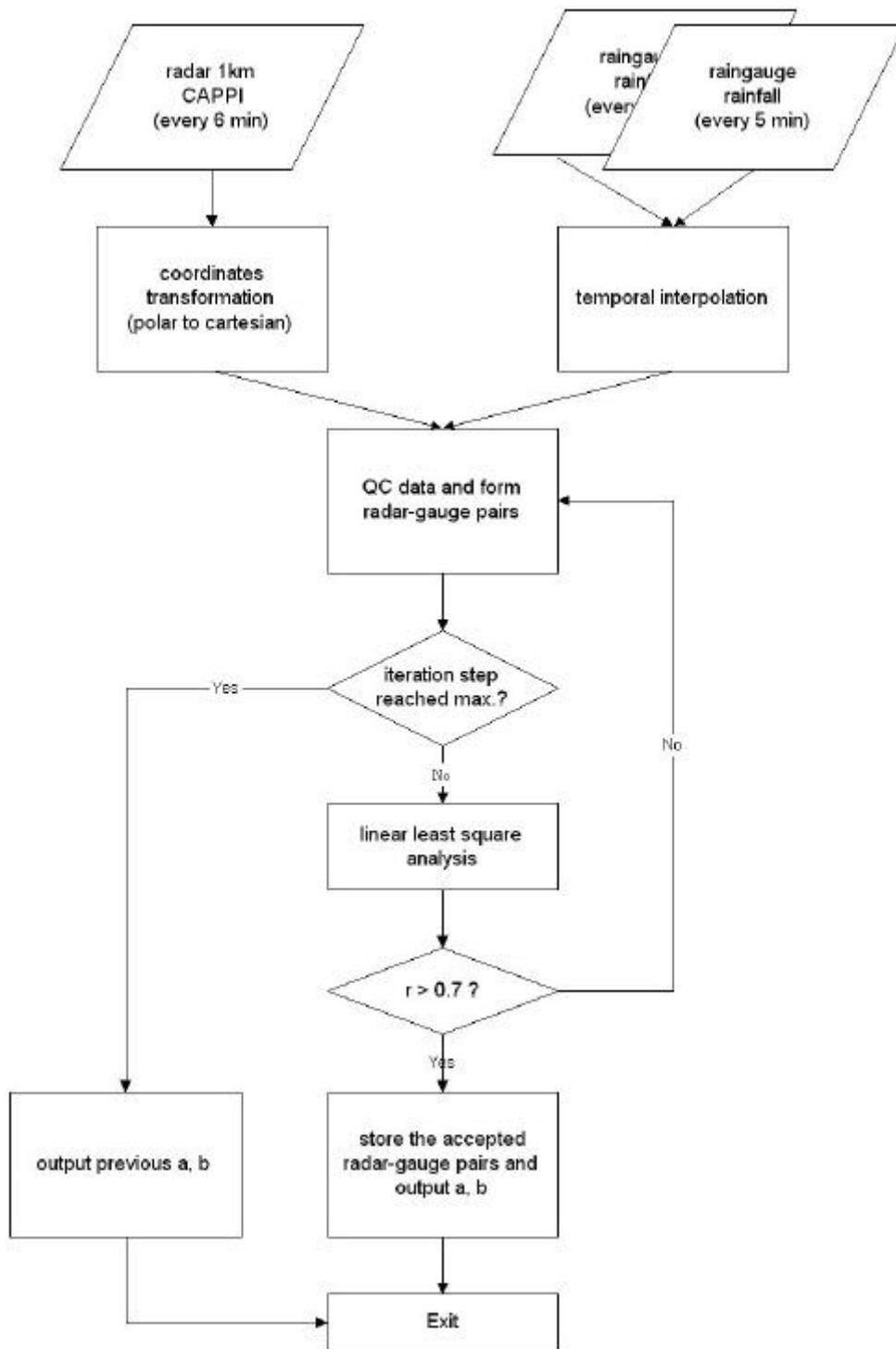
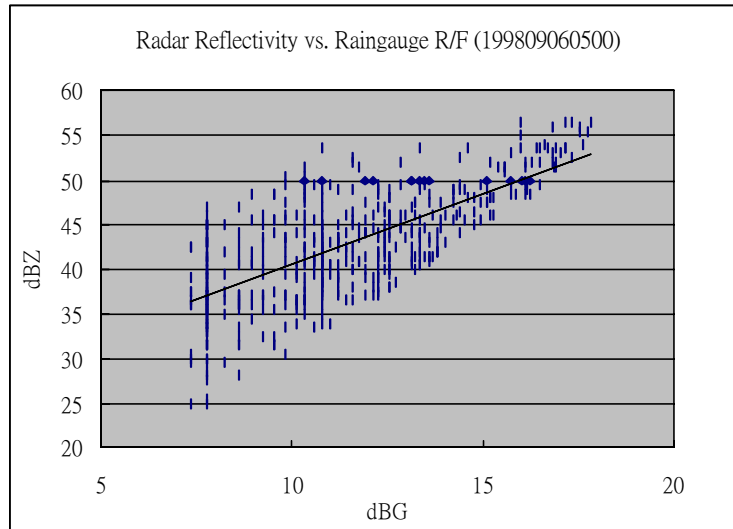


Figure 6 Flow diagram for the automatic radar-raingauge adjustment.

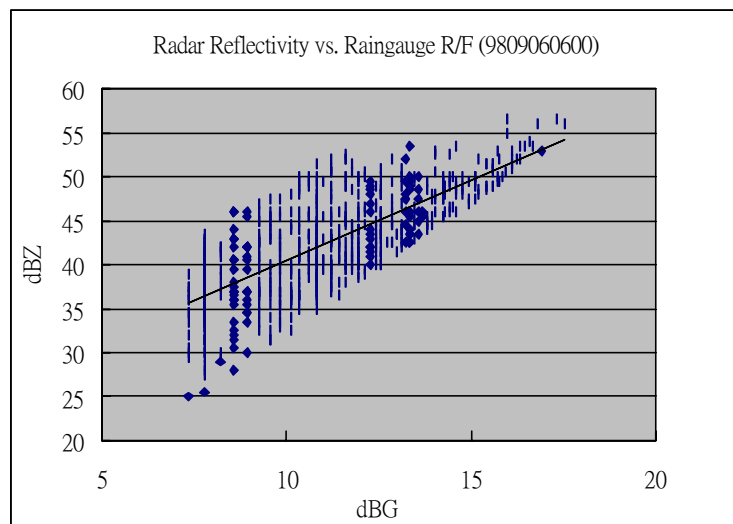
Case 1:	R(00)	↔	1	×	G(05)	+	1	×	G(10)
2:	R(06)	↔	4/5	×	G(10)	+	6/5	×	G(15)
3:	R(12)	↔	3/5	×	G(15)	+	7/5	×	G(20)
4:	R(18)	↔	2/5	×	G(20)	+	8/5	×	G(25)
5:	R(24)	↔	1/5	×	G(25)	+	9/5	×	G(30)
6:	R(30)	↔	1	×	G(35)	+	1	×	G(40)
7:	R(36)	↔	4/5	×	G(40)	+	6/5	×	G(45)
8:	R(42)	↔	3/5	×	G(45)	+	7/5	×	G(50)
9:	R(48)	↔	2/5	×	G(50)	+	8/5	×	G(55)
10:	R(54)	↔	1/5	×	G(55)	+	9/5	×	G(00)

Legend: R(24) means 6-minute reflectivity data with start time at 24 minutes past the hour
G(25) means 5-minute gauge data with end time at 25 minutes past the hour.

Figure 7 Matching of 6-minute radar reflectivity data with 5-minute rain gauge data (see explanation in text).



(a)



(b)

Figure 8 Scattered plots of radar-raingauge analysis for a rainstorm case on 9 June 1998. The parameters obtained from the least square analysis are: (a) at 5:00 HKT $a=395$, $b=1.5$, correlation coefficient=0.71; (b) at 6:00 HKT $a=258$, $b=1.6$, correlation coefficient=0.77.

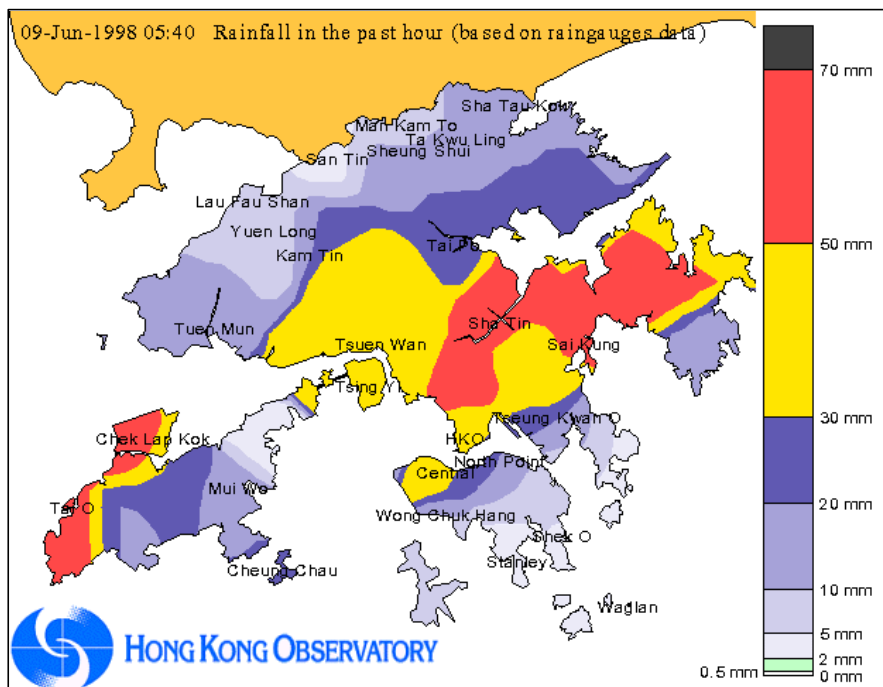
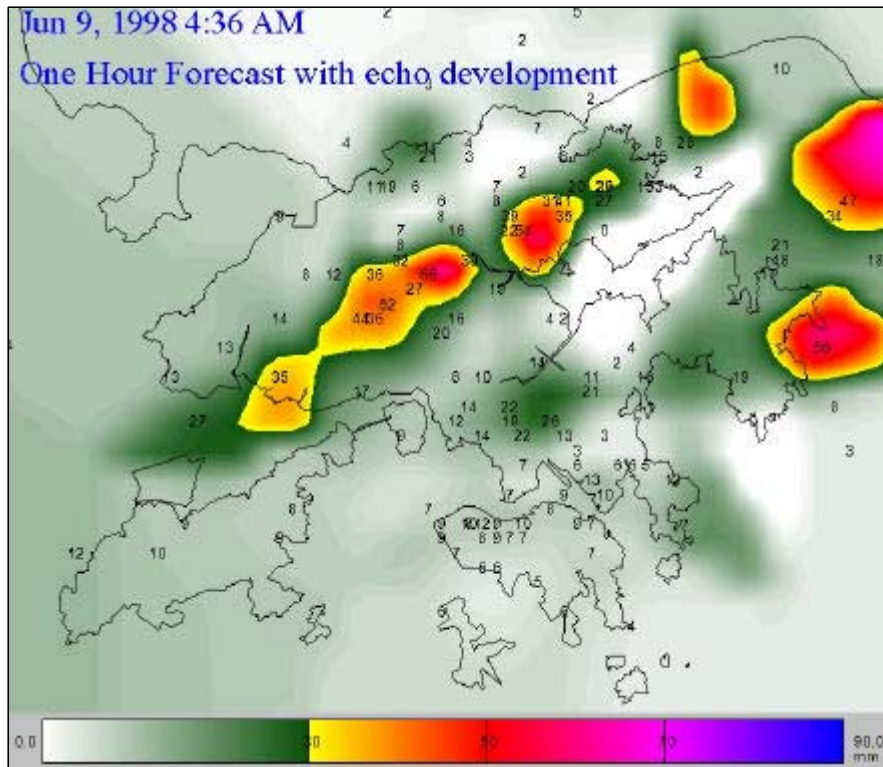


Figure 9 One hour rainfall forecast by SWIRLS issued at 4:36 HKT on 9 June 1998 (upper panel) and the corresponding one hour rainfall accumulation over the raingauges from 4:40 HKT to 5:40 HKT on 9 June 1998 (lower panel).

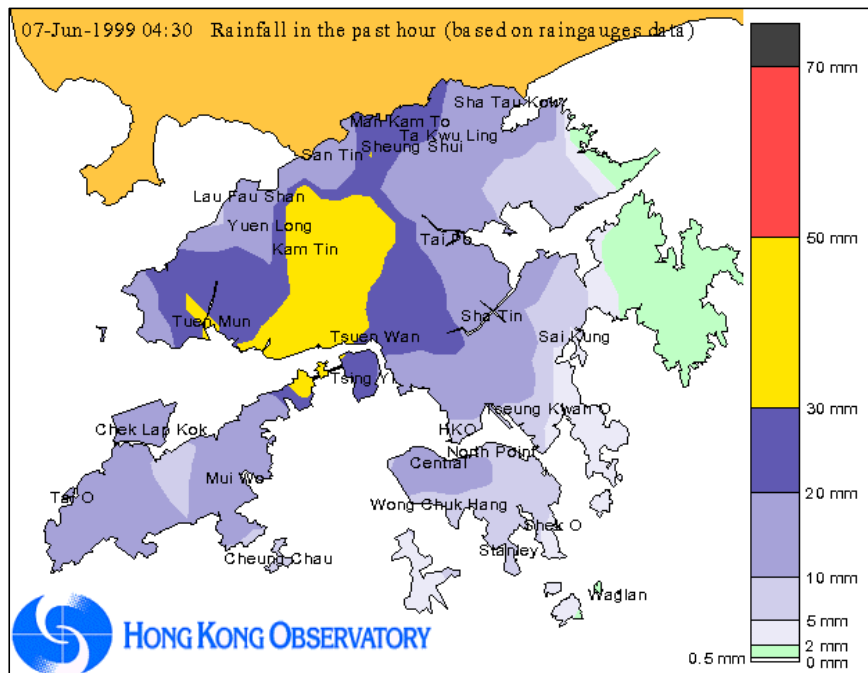
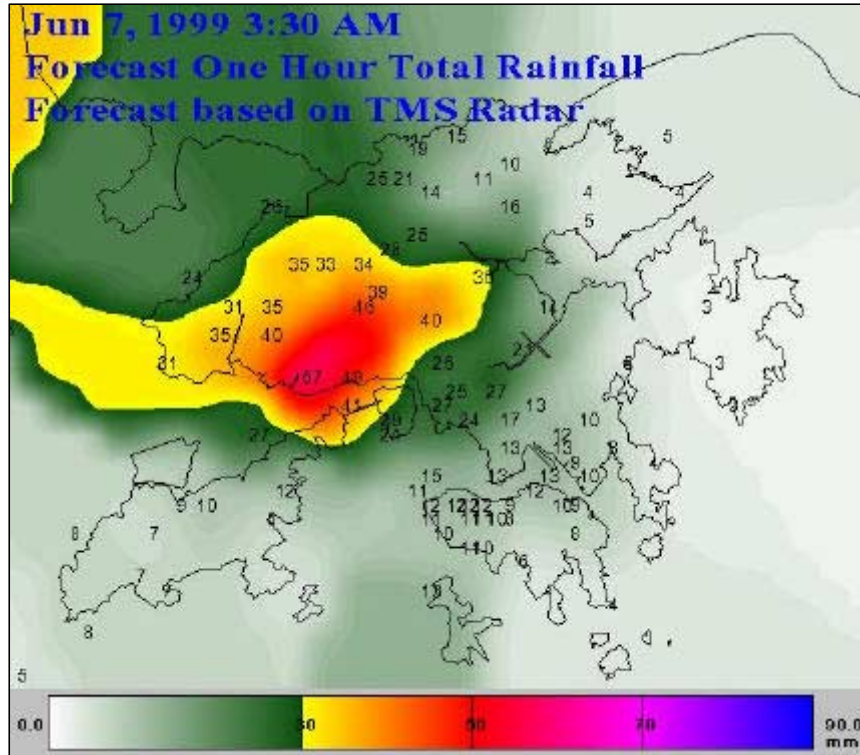


Figure 10 One hour rainfall forecast by SWIRLS for Typhoon Maggie issued at 3:30 HKT on 7 June 1999 (upper panel) and the corresponding one hour rainfall accumulation reported by the rain gauges from 3:30 HKT to 4:30 HKT on 7 June 1999 (lower panel).

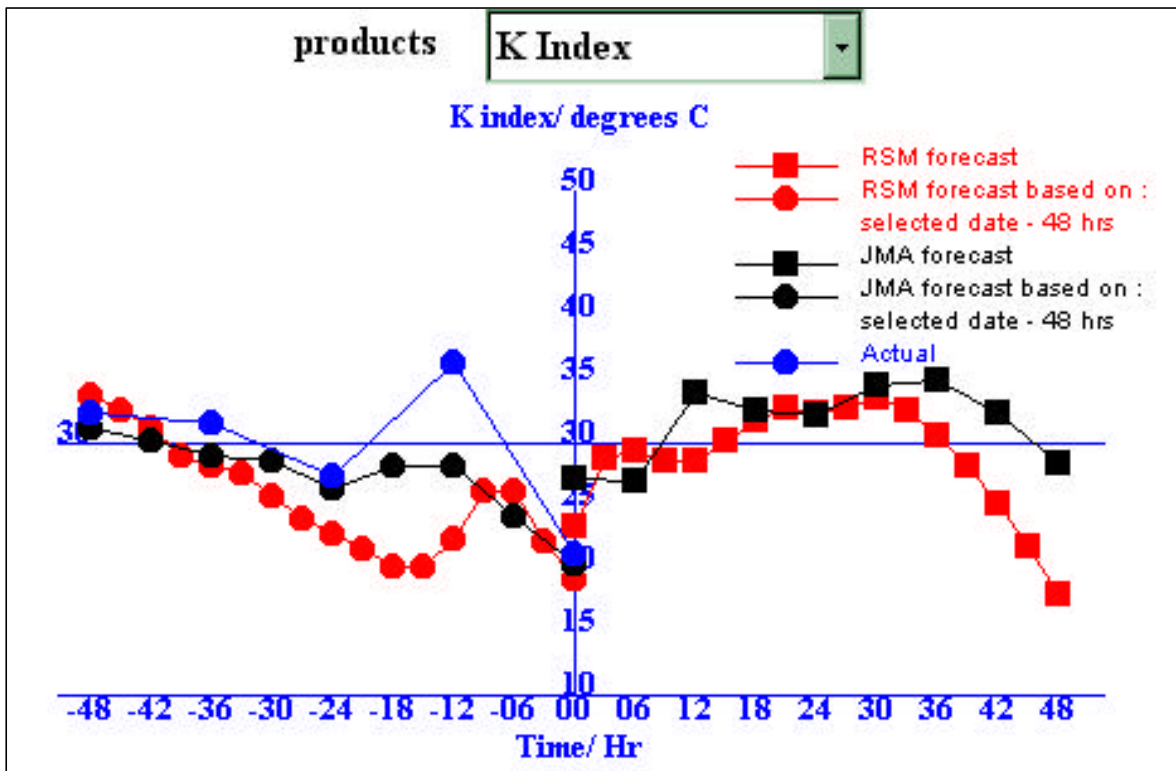


Figure 11 Time series display of instability indices in TephViewer

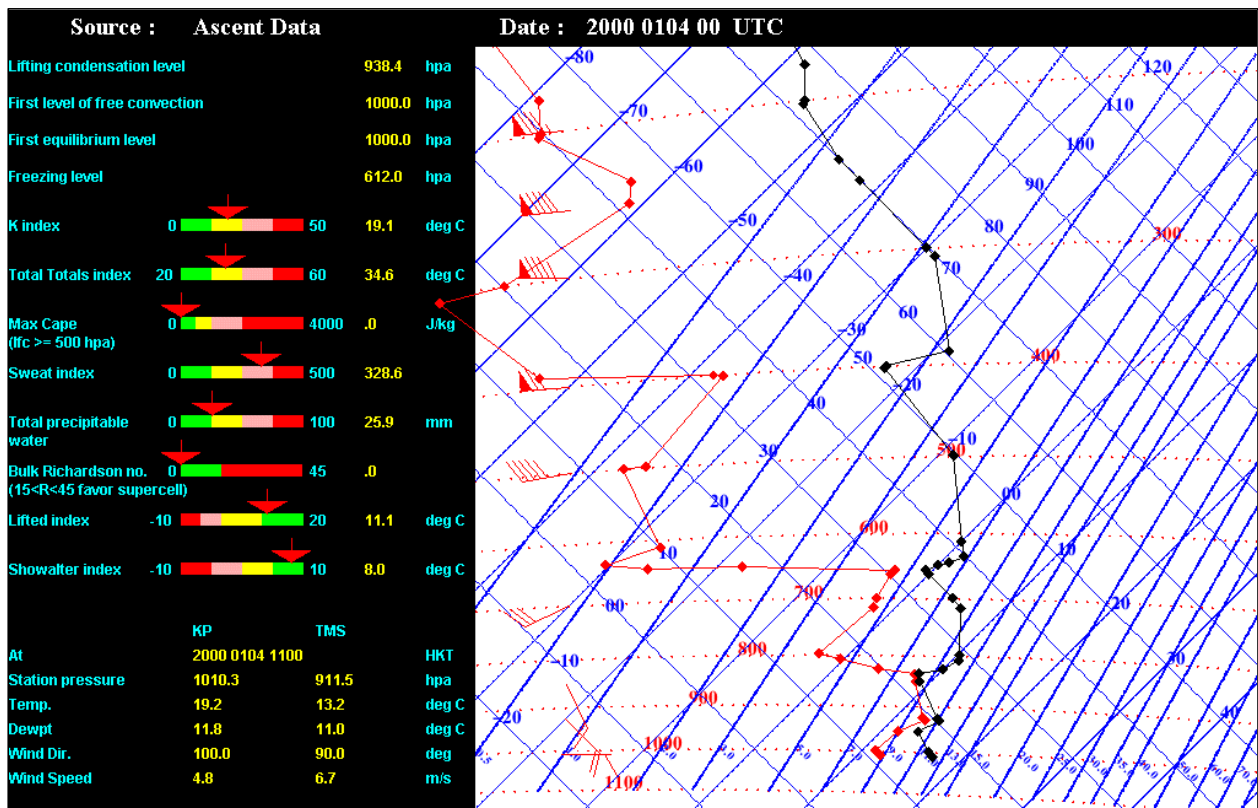


Figure 12 Tephigram plot in TephViewer with capability for interactive adjustment

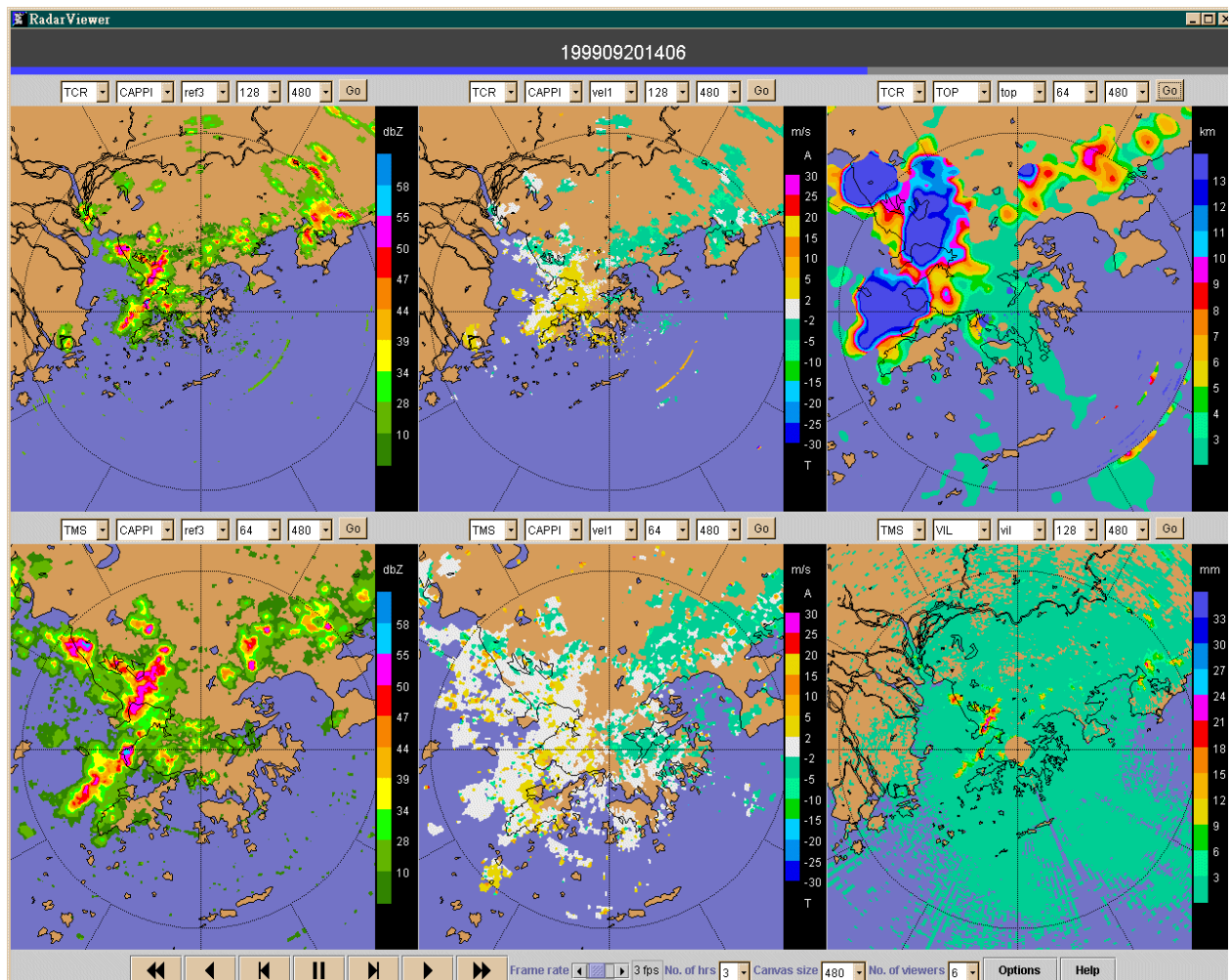


Figure 13 Synchronous display of radar products in RadarViewer

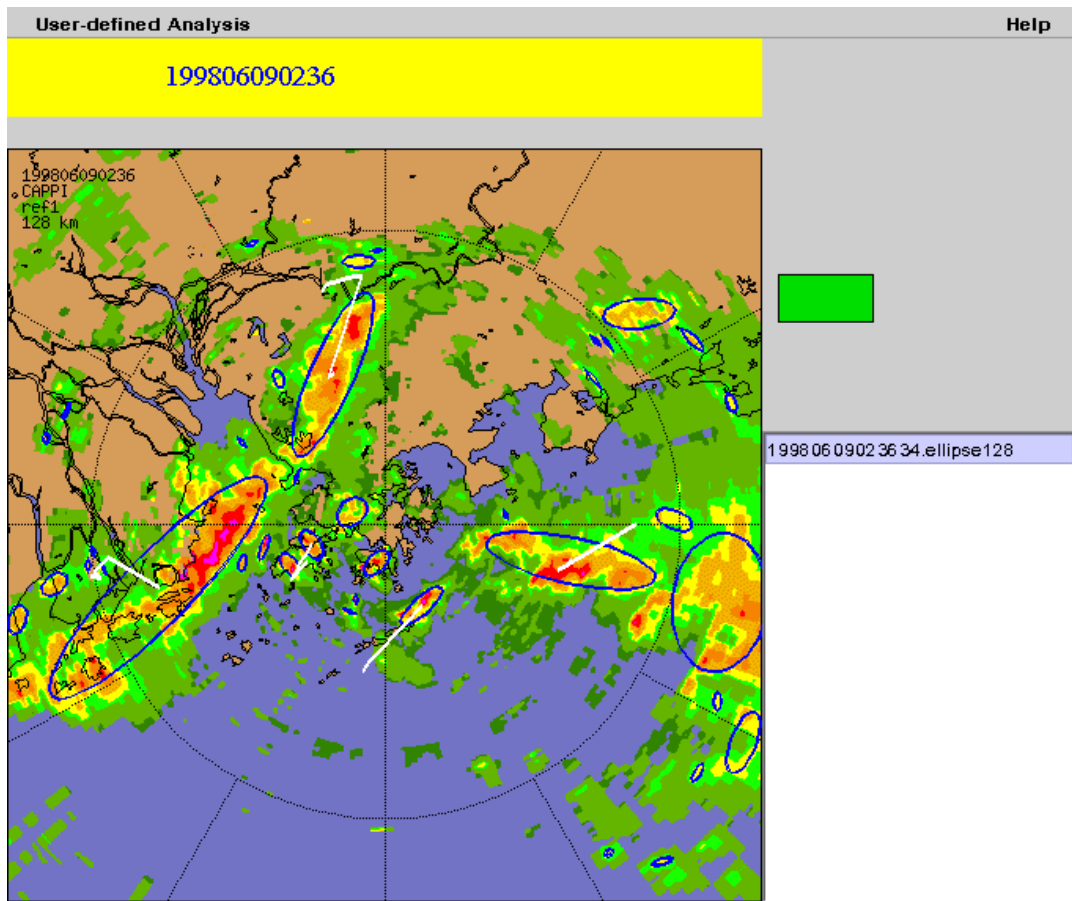


Figure 14 Complex interaction of echo groups on 9 June 1998 as revealed by the GTREC analysis. White lines connecting to centroids of ellipses indicate movement history of echo groups. One possible interpretation is that the SW-NE orientated squall line was moving southeastwards towards a slow-moving converging echo line lying just off the coast to the east of Hong Kong.